VEHICLE SYSTEM DYNAMICS, 2018
https://doi.org/10.1080/00423114.2018.1465574

A nonlinear model of bicycle shimmy

Nicolò Tomiati, Alessandro Colombo and Gianantonio Magnani

Department of Electronics, Information and Bioengineering (DEIB), Politecnico di Milano, Milan, Italy

ABSTRACT

This paper presents a nonlinear model accurately describing, both qualitatively and quantitatively, the onset and dynamics of bicycle shimmy. Methods of nonlinear dynamics, such as numerical continuation and bifurcation analysis, show that the model exhibits two stable periodic motions found experimentally in on-road tests: the weave and wobble (or shimmy) mode. The modelling results are compared with experimental data collected by riding a racing bicycle downhill at high speeds with hands on the handlebar. The model predicts with surprising accuracy the amplitudes and frequencies of the oscillations, the longitudinal velocity at which they occur, as well as the substantial independence of wobble frequency and amplitude from the forward speed. The lateral acceleration of the upper tube of the frame near the steering axis reaches 5–10 g, both in the model and in the data. The analysis shows that wobble onset and amplitude is particularly sensitive to changes in the torsional stiffness of the frame and strongly depends on tyre lateral force and aligning torque at the wheel–road contact point. It also allows to quantify the additional viscous rotary damping that should be added to the steering assembly to prevent wobble.

ARTICLE HISTORY
Received 24 November 2017
Revised 4 April 2018
Accepted 9 April 2018

KEYWORDS
Shimmy; wobble; nonlinear model; bifurcation analysis; bicycle; experimental data

1. Introduction

Wobble, more commonly known as *shimmy*, is an unwanted oscillation typical of bicycles and motorcycles. It is a high-frequency, often violent motion of the front frame with respect to the steering axis, addressed by popular journals and numerous videos on the Internet [1–3]. Such a phenomenon can have dramatic consequences, especially for the unprepared rider. Although shimmy is well-known and documented in the scientific literature, little on-road data is available for a thorough study of the phenomenon.

One of us experienced several scary shimmies, riding downhill at high speed with hands on the handlebar, first with an aluminium alloy frame and then with a carbon professional racing bicycle. Once the carbon bicycle was sensorised, we discovered that lateral accelerations on the horizontal tube of the frame were in the range of 5–10 g, as can be seen in Figure 1(a). These data were collected in August 2014 near Lecco (Italy) and give unique information about wobble amplitude, duration, phase and dependence on forward speed.

CONTACT Nicolò Tomiati nicolo.tomiati@polimi.it

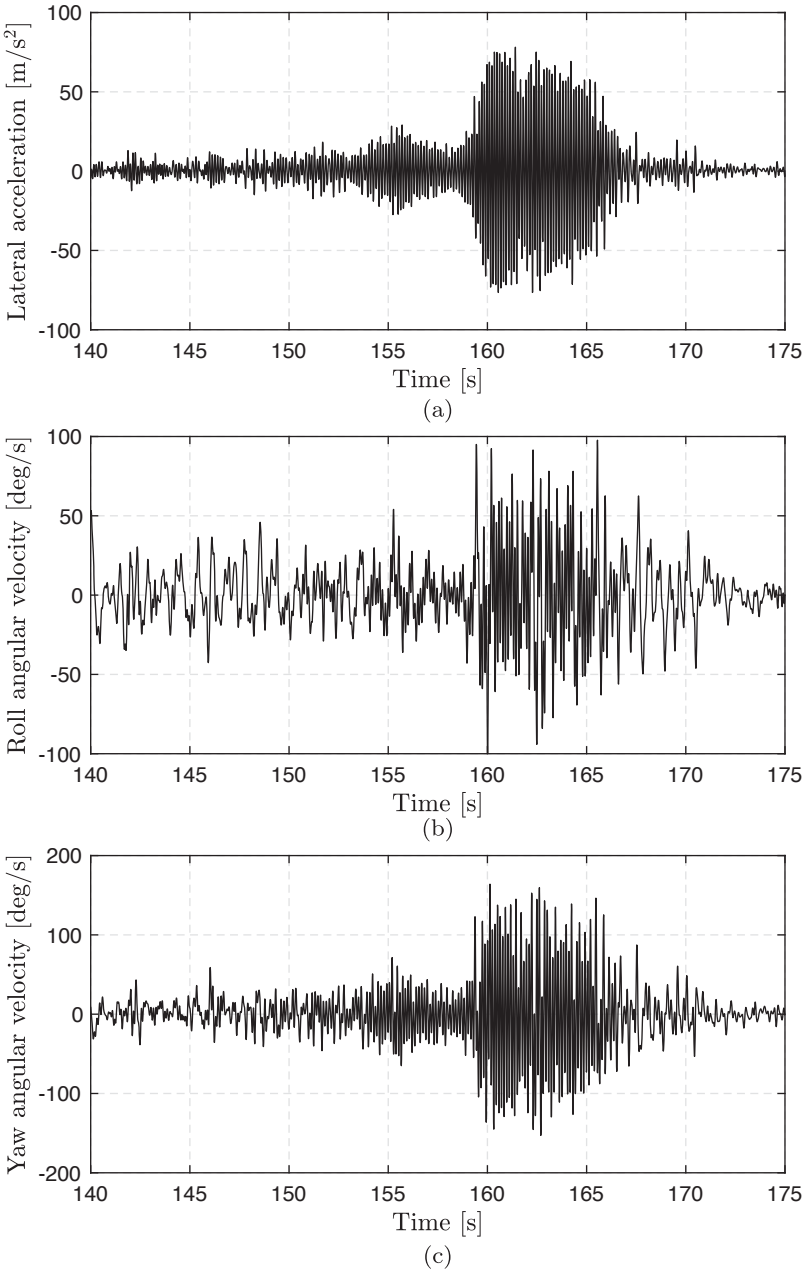

Figure 1. Data recorded by an IMU on the rear frame of the racing bicycle near the steering axis. Test activity of August 2014. (a) Lateral acceleration, (b) roll angular velocity, (c) yaw angular velocity.

A couple of years before, in 2011, another on-road test activity was performed by the same rider and with the same carbon bicycle. The results of this activity are described in [4]. This was the starting point of our studies on what causes shimmy and how it can be fought, and inspired other works such as [5,6].

To make use of the available data, we needed a suitable model of the bicycle: sufficiently simple to link the observed phenomena with meaningful physical quantities, but sufficiently detailed to capture as much as possible the complex dynamics we found in the data. Perhaps surprisingly, given the apparent simplicity of a bicycle, a definitive model capturing even just its macroscopic dynamics has still not been found, unless one considers the complex multi-body models that offer highly detailed numerical simulations but little insight into the physical origins of the observed phenomena. In this paper, starting from the dataset collected in Lecco we propose for the first time a model capable of making sense of the data, both qualitatively and quantitatively.

The foundation of our model is the three degrees of freedom Carvallo–Whipple model illustrated in [7]. It consists of four rigid bodies connected by rotational joints: rear wheel, rear frame with a passive rigid rider, front frame and front wheel. It stands on the assumption of ideal rolling between wheels and road surface, with no lateral and longitudinal slip. This model highlights two important vibrational modes that characterise a two-wheeled vehicle: *weave* and *capsize*. Weave is an oscillatory motion of the rear frame about roll axis together with oscillations about the yaw axis. It is a low-frequency mode that can be easily counteracted by the rider. Capsize is a non-oscillatory motion by which the bicycle follows a spiral path with increasing values of the roll angle, ultimately leading to a lateral fall. No oscillation related to shimmy is observed in this model.

Subsequent studies on motorcycle dynamics [8–10] have shown that three new components are needed to trigger wobble, and they are believed to jointly contribute to determine shimmy: an additional degree of freedom, which represents the lateral rotation of the front frame about the axis β [5,11], a non-ideal characteristic of tyre lateral force and aligning torque, and a non-trivial dynamics of the tyres. In fact, during motion tyres do not respond instantaneously upon moving from the equilibrium condition, but it takes some time before lateral force and aligning torque approach the final value. The importance of tyres dynamics in shimmy was first asserted in [12].

The onset of wobble mode was partially explained with a linear bicycle model in [6], based on the Carvallo–Whipple model with the addition of the effects highlighted above. The linear model displayed a Hopf bifurcation with eigenvalues compatible with the frequency of shimmy. Shimmy is, however, a stable periodic motion, and as such it is an essentially nonlinear phenomenon. The linear model of [6] cannot capture its dynamics (and in particular cannot describe its amplitude, for validation against experimental evidence) nor can it describe the complex interaction of the shimmy oscillation with other stable but non-equilibrium riding regimes.

In this work we extend the linear model of the racing bicycle described in [6], adding the nonlinear terms that are necessary to describe, qualitatively and quantitatively, the onset as well as the dynamics of shimmy. To this end, we have relaxed the assumption of small angles at the contact point between wheel and road surface. The numerical analysis of our nonlinear model closely matches the experimental results described in Figure 1 and in [4], and the outputs of a complex multi-body model illustrated in [13]. This means that the model presented in this work is an effective mathematical tool to interpret the experimental data. Moreover, and most importantly, it allows to study and understand shimmy, without riding the bicycle downhill at high speed – a frightening and dangerous experience for the rider. The methods we use in this paper – a nonlinear model and bifurcation analysis – closely resemble those used in [14]. That work is however addressing a motorcycle

model, rather than a bicycle, and the results are not tested against experimental data as we do here.

The paper is organised as follows. Section 2 gives an overview of the bicycle model and provides a detailed description of the nonlinearities introduced in the model. In Section 3 the nonlinear analysis is performed. The starting points are time simulations and frequency spectra of the system for different parameter values. Then, a one-parameter continuation in the forward speed and a two-parameter bifurcation diagram in the plane of forward velocity and torsional frame stiffness are computed. Section 4 is devoted to understanding the influence of a steering damping on the vibrational modes. Finally, Section 5 summarises and discusses the results.

2. Model description

The linear racing bicycle model on which this work is based is taken from [6], where parameters were in turn identified using the same bicycle as in Figure 1. The authors of [6] modelled different possible configurations: passive rider with hands off the handlebar and in an upright position, rider with hands off the handlebar and upper body leaning forward and, lastly, rider with hands on the handlebar and upper body leaning forward. These different rider's positions change the loads distribution, the location of the centre of gravity and the inertia tensors. For our purpose, the most interesting configuration is the last one: it matches the set-up of the on-road experiments of Figure 1, and is the most common when riding a racing bicycle at high speed, when shimmy is more likely to occur. For this reason, this paper will only focus on the model of a rider with hands on the handlebar and upper body leaning forward.

The bicycle model is illustrated in Figure 2. It is a five-degrees-of-freedom system with a passive rider model, lumped masses and spring-damper elements. The origin of the horizontal moving reference frame is the rear contact point between wheel and road. The main frame of the bicycle, which includes the vehicle rear part, the rider and the rear wheel, can rotate about the vertical axis z with an angular velocity $\dot{\psi}$. At the same time it can

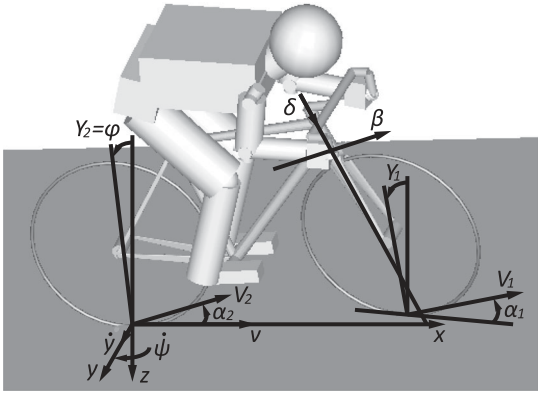

Figure 2. Rider with hands-on the handlebar and with his upper body bent forward. Reference system and degrees of freedom are shown with their positive values. Data are taken from [6].

rotate about the roll axis x, which is included in the longitudinal symmetry plane, with an angle φ. Another degree of freedom is the lateral displacement y of the rear contact point. The forward speed v is constant and set as a model parameter. The front frame, that is, the assembly of handlebar, stem, fork and front wheel, is connected to the rear part by a rotational joint. This element allows rotations about the steering axis δ. The model also takes into account rotations of the front frame about the axis β. This axis is in the symmetry plane of the vehicle and is perpendicular to the head tube. This additional generalised coordinate is restrained by a spring-damper element and allows to model the lateral compliance of the rear frame at the head tube and of the fork, and the lateral movement of the front hub [15].

We do not report here the equations of the model in Figure 2, as these can be found, with more detailed model description, in [6]. We now focus instead on the changes introduced in the model considered here compared to the one found in [6].

2.1. Model nonlinearities

The contact area between road and wheel is a region that depends on tyres inflation pressure and geometry. Under normal operating conditions the resulting force is usually shifted backwards with respect to the ideal contact point by a distance called pneumatic trail. This results in a torque at the ideal contact point, as shown in Figure 3 using the sign convention from [16].

The relation between the camber and side-slip angles[1] and the (normalised) lateral force F_y and self-aligning torque M_z, under the assumption of straight rectilinear motion, is captured by the following equations:

$$\bar{F}_y = \frac{F_y}{F_z} = \bar{F}_{\text{camber}}(\gamma) + \bar{F}_{\text{sideslip}}(\alpha), \tag{1}$$

and

$$\bar{M}_z = \frac{M_z}{F_z} = \bar{M}_{\text{twisting}}(\gamma) + \bar{M}_{\text{selfaligning}}(\alpha), \tag{2}$$

where F_z is the vertical load acting on the wheel.

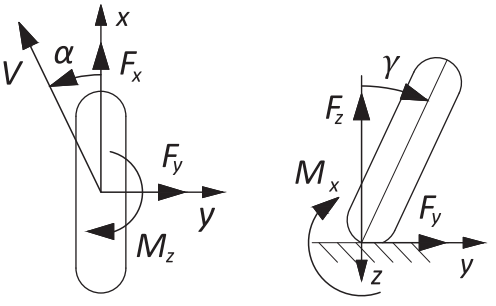

Figure 3. Tyre definition: camber angle γ is the angle between the wheel centre plane and the vertical axis z of the road surface. Side-slip angle α is the angle between the wheel centre plane and the direction of its velocity V . F_x is the longitudinal force, F_y is the lateral force and F_z is the normal force. M_x is the overturning torque and M_z is the aligning torque. Positive values are shown. The left figure is a top view, the right one is a rear view.

The above equations appear in the model in [6] where, standing on a small-angles assumption, the functions $\bar{F}_{\text{camber}}$, $\bar{F}_{\text{sideslip}}$, $\bar{M}_{\text{twisting}}$, $\bar{M}_{\text{selfaligning}}$ are taken linear:

$$\bar{F}_{\text{camber}}(\gamma) = C_{\text{f}\gamma}\gamma, \quad \bar{F}_{\text{sideslip}}(\alpha) = C_{\text{f}\alpha}\alpha, \tag{3a}$$

$$\bar{M}_{\text{twisting}}(\gamma) = C_{\text{m}\gamma}\gamma, \quad \bar{M}_{\text{selfaligning}}(\alpha) = C_{\text{m}\alpha}\alpha. \tag{3b}$$

The coefficients of the linear functions used in [6] are reported in Table 1. The self-aligning torque tends to align the wheel to the direction of speed; on the other hand, the twisting torque represents the tendency of the cambered wheel to move along a trajectory with a smaller curvature radius, thus it has a completely different effect than the self-aligning torque. It is worth noting that all the coefficients in Equations (3) may be different for the front and the rear wheel. In the remainder of this work it will be assumed that both wheels have the same elastic properties.

Additionally, the camber and side-slip angles themselves exhibit a dynamic behaviour, due to the delayed response of the wheel under non-zero side-slip or camber angles. This delay in the deformation is modelled by two first-order differential equations of the form[2]:

$$\frac{\sigma_\alpha}{v}\dot{\alpha} + \alpha = \hat{\alpha}, \tag{4}$$

$$\frac{\sigma_\gamma}{v}\dot{\gamma} + \gamma = \hat{\gamma}, \tag{5}$$

where $\hat{\alpha}$ and $\hat{\gamma}$ are functions of the state variables $\beta, \delta, \varphi, y, \psi$ and their time derivatives, as reported in [6]. The characterising parameter describing this effect is the relaxation length σ. This is a constant in the above equations, though a model with σ depending on side-slip and camber angles would be more accurate. Its value can be determined experimentally, as stated in [17].

We know from real-world experience that, even during a violent shimmy, the rotations about roll, yaw, steering, and β axes have limited amplitude. For example, during our on-road tests we observed a roll angle $|\varphi| \leqslant 3^\circ$, and a yaw angle $|\psi| \leqslant 4.5^\circ$. Small rotations, however, do not necessarily translate into small deformation at the contact points between tyres and road surface, especially at the front wheel: the resultant tyre strain is an algebraic sum of the deformation caused by rotations around axes δ, β, ψ and φ and their time derivatives. To account for the nonlinear effects of tyre deformation in the model, we dropped the assumption of small camber and side-slip angles, and adopted a realistic tyres description.

Typical trends of the terms $\bar{F}_{\text{camber}}$, $\bar{F}_{\text{sideslip}}$, $\bar{M}_{\text{twisting}}$, and $\bar{M}_{\text{selfaligning}}$ are found in [18]. That work reports the characteristics of different tyres under multiple operating conditions,

Table 1. Coefficients used to determine forces and torques in the linear case.

Coefficient	Value	Unit
$C_{\text{f}\gamma}$	0.8594	rad^{-1}
$C_{\text{f}\alpha}$	13.7510	rad^{-1}
$C_{\text{m}\gamma}$	0.0344	m rad^{-1}
$C_{\text{m}\alpha}$	−0.3438	m rad^{-1}

but none of them is a racing tyre. Racing tyres, which were used in the test of Figure 1, have a significantly different structure than other tyre types. To better approximate the conditions found in our field test in terms of steady-state force and moment characteristics, and lacking a precise identification of the tyres used in the test, we modelled our nonlinear characteristics to have the same trend as in [18], but using data for the racing tyre Vittoria Randonneur Hyper 37-622, taken from [19].

As seen in [18], the camber force saturates at high values of the camber angle. We model this saturation with a hyperbolic tangent, obtaining the following formula for the normalised camber force:

$$\bar{F}_{\text{camber}} = A_1 \tanh\left(\frac{C_{\text{f}\gamma}\,\gamma}{A_1}\right). \tag{6}$$

Similarly, with increasing angles the lateral force and the twisting torque level off from the tangent stiffness due to the slippage in the contact area. Hence, we choose to model the second term of the lateral force and the twisting torque as:

$$\bar{F}_{\text{sideslip}} = A_2 \tanh\left(\frac{C_{\text{f}\alpha}\,\alpha}{A_2}\right), \tag{7}$$

$$\bar{M}_{\text{twisting}} = A_3 \tanh\left(\frac{C_{\text{m}\gamma}\,\gamma}{A_3}\right). \tag{8}$$

The trend of the self-aligning torque is significantly different from the three functions above: it has negative slope at very low side-slip angles, a local minimum at small angles, and a constant asymptote for large angles. We describe this behaviour with the formula:

$$\bar{M}_{\text{selfaligning}} = A_4 \sin(A_5 \tanh(A_6\alpha)), \tag{9}$$

which is very similar to the simplified *Magic Formula* provided by Pacejka [16] to represent the same characteristic. Parameter A_4 is the peak factor and, for $A_5 > \pi/2$, represents the minimum of the curve. The aligning stiffness $C_{\text{m}\alpha}$, which is the derivative of (9) at $\alpha = 0$ and appears as an explicit parameter in [6], is here a function of A_4, A_5, A_6, with value:

$$C_{\text{m}\alpha} = A_4 A_5 A_6. \tag{10}$$

Using Equations (6)–(9) in (1) and (2) we finally obtain:

$$F_{\text{y}} = \left[A_1 \tanh\left(\frac{C_{\text{f}\gamma}\,\gamma}{A_1}\right) + A_2 \tanh\left(\frac{C_{\text{f}\alpha}\,\alpha}{A_2}\right)\right] F_z, \tag{11}$$

$$M_z = \left[A_3 \tanh\left(\frac{C_{\text{m}\gamma}\,\gamma}{A_3}\right) + A_4 \sin(A_5 \tanh(A_6\alpha))\right] F_z. \tag{12}$$

Table 2 reports the values of the parameters used in our numerical analysis. Note that we have taken parameter values so that the slopes of (11) and (12) at $\alpha = 0$ and $\gamma = 0$ coincide with the stiffness coefficients used in [6] and found in Table 1. Figure 4 highlights the difference between linear and nonlinear tyre characteristics for the four components of normalised lateral force and aligning torque.

Table 2. Parameters used to determine forces and torques in the nonlinear case.

Coefficient	Value	Unit
A_1	0.7000	–
A_2	0.6200	–
A_3	0.0400	m
A_4	−0.0090	m
A_5	3.2300	–
A_6	11.8258	–

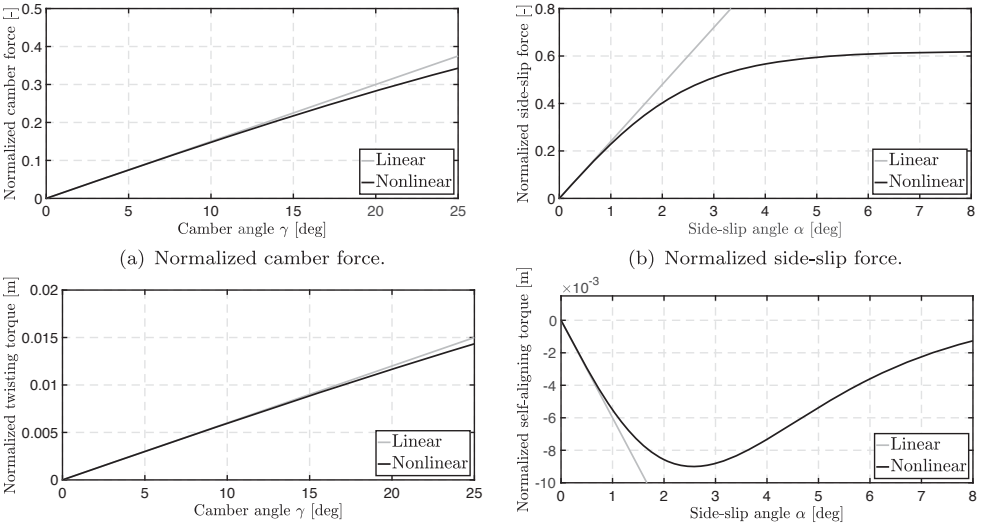

(a) Normalized camber force.

(b) Normalized side-slip force.

(c) Normalized twisting torque.

(d) Normalized self-aligning torque.

Figure 4. Differences between linear and nonlinear tyre characteristics. First row: lateral force F_y; second row: aligning torque M_z.

3. Nonlinear dynamics of the racing bicycle

We now discuss the dynamics and bifurcations of our bicycle model. Bifurcation analysis was performed using MatCont [20], a free graphical Matlab software package for the interactive numerical study of dynamical systems, which allows to simulate the system and, most importantly, to track bifurcations of its attractors as one or more parameters are changed.

In our model the two most significant parameters are the forward speed v and the torsional stiffness coefficient k_β. The latter represents the lumped compliance at the steering head related to rotations about the β-axis, and can be partially modified by stiffening the bicycle frame during experimental test activities. The purpose of the analysis that follows is to describe how the main attractors of our model, that is, the main dynamic regimes which we expect to observe in the model after all transients have vanished, depend on these two parameters. In particular, we analyse the relative contributions of the two main vibrational modes of the bicycle (weave and wobble) to the overall dynamics, showing that they closely match, quantitatively and qualitatively, the data obtained in the tests of Figure 1.

3.1. Time and frequency domain analysis

Let us start by simulating the bicycle's behaviour at three different speeds. In all simulations, we set the stiffness parameter $k_\beta = 4784.2$ Nm/rad, matching the value estimated in [6] for the bicycle used in the experiments of Figure 1.

Figure 5(a,b) shows the trajectories of δ, β, $\dot{\varphi}$, and $\dot{\psi}$ when $v = 13.5$ m/s, while Figure 5(c) shows the corresponding spectra computed by a fast Fourier transform. At this speed value, the bicycle has an unstable equilibrium where all angles are zero. An arbitrarily small perturbation from this equilibrium brings the system onto a stable and constant-amplitude low-frequency oscillation that mainly involves the rear frame: the bicycle is oscillating about the yaw and roll axes. This is typical of the weave mode of vibration.

Figure 5(a) shows that the roll and yaw angular velocities have a phase difference of 90°: when the former is zero, the latter reaches its extrema. From the point of view of the rider, the oscillation starts with a positive (clockwise) rotation of the steering axis, which causes the bicycle to rotate clockwise about the yaw axis. This is then followed by a counter-clockwise rotation about the roll axis. The amplitude of the roll oscillation is larger than that of the yaw one. These results are in accordance with the data reported in [13], where a high-definition multi-body model of the racing bicycle is used to simulate its dynamics. The frequency of the weave at the selected combination of forward speed and frame stiffness is equal to 0.91 Hz (Figure 5(c), the others peaks are signal harmonics). This value is consistent with those recorded during the experimental activity of Figure 1.

A qualitatively different oscillation is found in Figure 6 for $v = 14.1$ m/s, a speed only slightly higher than the previous case. The trajectories now exhibit a mix of both low-frequency and high-frequency, non-harmonic components, respectively, at 0.93 and 7.75 Hz. This means that the weave mode is still visible, with slightly higher frequency than before, while a new high-frequency mode has emerged.

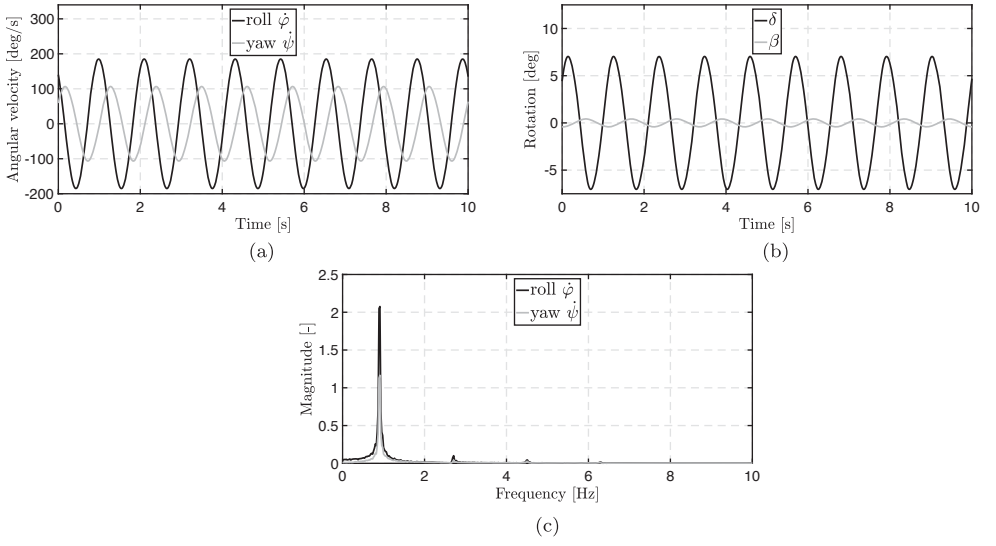

Figure 5. Simulation for $v = 13.5$ m/s and $k_\beta = 4784.2$ Nm/rad. (a) Trajectories of roll $\dot{\varphi}$ and yaw $\dot{\psi}$ angular velocities, (b) trajectories of rotations δ and β, (c) corresponding spectra.

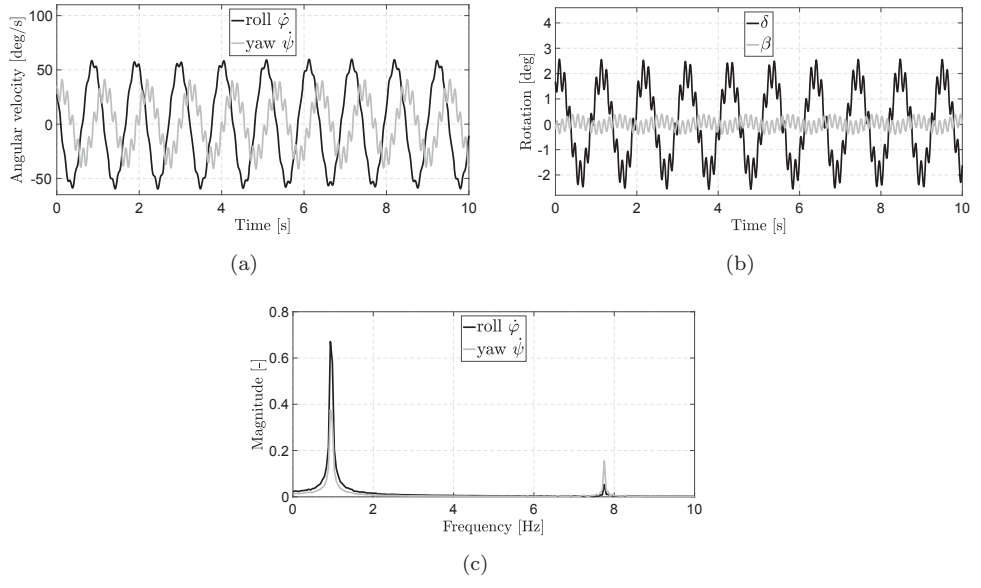

Figure 6. Simulation for $v = 14.1$ m/s and $k_\beta = 4784.2$ Nm/rad. (a) Trajectories of rotations δ and β, (b) trajectories of roll $\dot{\varphi}$ and yaw $\dot{\psi}$ angular velocities, (c) corresponding spectra.

Finally, Figure 7 depicts the bicycle's behaviour at $v = 15$ m/s. In this case, the amplitude of the yaw angular velocity is greater than the roll one. Moreover, the two signals are in antiphase: when the former reaches a maximum, the latter is at its minimum. This phase difference is a distinctive property of the wobble mode, in accordance with the output of

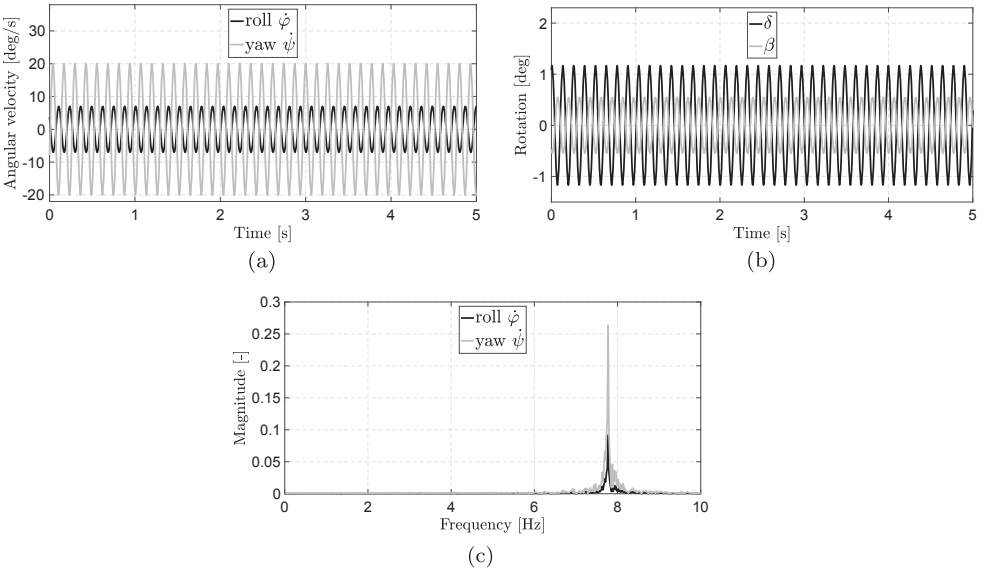

Figure 7. Simulation for $v = 15$ m/s and $k_\beta = 4784.2$ Nm/rad. (a) Trajectories of roll $\dot{\varphi}$ and yaw $\dot{\psi}$ angular velocities, (b) trajectories of rotations δ and β, (c) corresponding spectra.

the multi-body model in [13]. Figure 7(b) shows the trajectory of the steering and β axes: their amplitude and their frequency are consistent with a wobble mode. When the front frame rotates clockwise about the head tube (positive value), the rotation about β axis is such that the bicycle tries to keep the direction of the straight motion. This is due to the contact constraint between front wheel and road surface. The frequency of the main peak is 7.77 Hz (Figure 7(c)) and it is quite close to the 7.5 Hz recorded during the test activity of Figure 1. Note that the high-frequency peak that we found in Figure 6(c) (centred at 7.75 Hz) is very close to the frequency peak of the wobble mode in Figure 7, and the phase of yaw and roll signals are approaching a 180° offset. This suggests that the high-frequency peak of Figure 6(c) is a wobble mode, interplaying with the more prominent weave mode.

Summarising the results obtained in this section, for low values of the forward speed the only mode of vibration that characterises the bicycle is the weave, while for high values of the speed there is only wobble. In between there is a speed interval in which the two vibrational modes coexist and interact.

3.2. One-parameter bifurcation analysis

To better characterise the interaction between weave and wobble modes, identified in the previous section, we now report a one-parameter bifurcation analysis of our model using the forward speed v as bifurcation parameter, keeping the torsional stiffness coefficient constant and equal to $k_\beta = 4784.2$ Nm/rad. By changing v in the interval $5 \leqslant v \leqslant 25$ m/s, which are typical operating conditions for a racing bicycle, we identify and numerically continue the equilibria and limit cycles of our model, showing how they transform into one another. Figure 8 summarises the results of the numerical continuation with a zoom to better understand the label of the points. Subfigures illustrate the maximum amplitude of the state variables δ, β, $\dot{\psi}$ and $\dot{\varphi}$. Solid lines stand for branches of stable solutions (equilibria or limit cycles), whereas dashed branches stand for unstable solutions.

The straight line at the bottom of all four subfigures is the trivial equilibrium, that is, the rectilinear motion of the bicycle. It is unstable over the whole speed interval. The equilibrium undergoes two supercritical[3] Hopf bifurcations, identified by points $\mathrm{H_{wo}}$ at $v = v_{\mathrm{Hwo}} = 13.23$ m/s and $\mathrm{H_{we}}$ at $v = v_{\mathrm{Hwe}} = 14.21$ m/s.

At $\mathrm{H_{wo}}$, an unstable limit cycle is born from the equilibrium. As we can see in the figures, the limit cycle exists for $v > v_{\mathrm{Hwo}}$, and becomes stable through a supercritical Neimark–Sacker bifurcation (point $\mathrm{NS_{wo}}$ at $v = v_{\mathrm{NSwo}} = 14.23$ m/s). For $v > v_{\mathrm{NSwo}}$, this stable limit cycle appears to be the only attractor of the system. This is the wobble oscillation we identified in the previous section. For $v < v_{\mathrm{NSwo}}$, the supercritical Neimark–Sacker bifurcation marks the birth of a stable torus, which is a periodic or quasi-periodic attractor characterised by oscillations at two distinct frequencies. This is, most likely, the origin of the mixed weave-wobble oscillation we found by simulation.

At $\mathrm{H_{we}}$, the supercritical Hopf bifurcation marks the birth of an unstable limit cycle with the frequency characteristics of the weave motion. This becomes stable through a Neimark–Sacker bifurcation (point $\mathrm{NS_{we}}$ at $v = v_{\mathrm{NSwe}} = 14.11$ m/s). This Neimark–Sacker bifurcation, at a speed only slightly lower than v_{NSwo}, also marks the disappearance of the stable torus generated at $v = v_{\mathrm{NSwo}}$. The amplitude of the weave limit cycle, in δ and β, rapidly changes in v.

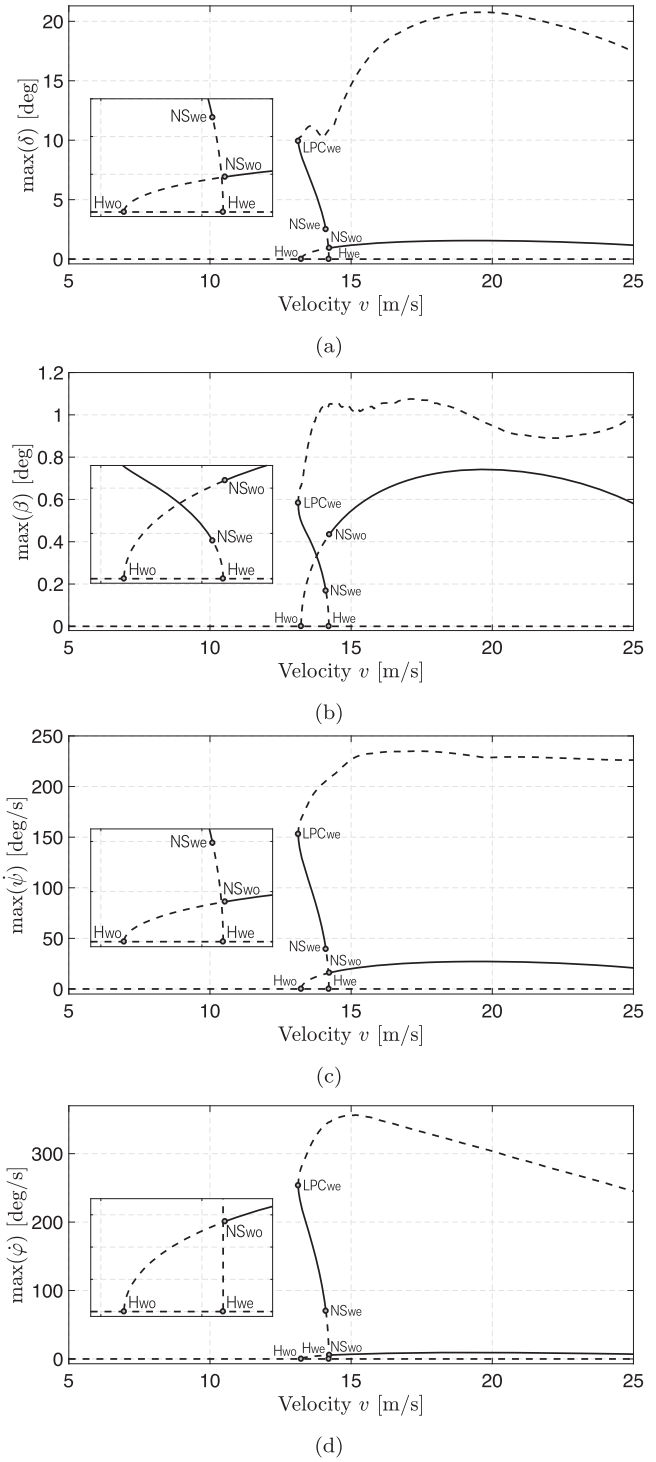

Figure 8. One-parameter continuation in v for $k_\beta = 4784.2$ Nm/rad. (a) Steering rotation δ, (b) β angle, (c) yaw angular velocity $\dot{\psi}$ and (d) roll angular velocity $\dot{\varphi}$. Solid curves represent stable parts of branches, whereas dashed lines stand for unstable parts. Points labelled with H are Hopf bifurcations, NS are Neimark—Sacker bifurcations (tori) and LPC are limit point of cycles.

At velocity $v < v_{\mathrm{LPCwe}} = 13.13$ m/s, the weave cycle loses stability through a fold bifurcation, and below this speed we did not find any other attractor: any initial condition out of the equilibrium eventually diverges to infinity.

Overall, the model exhibits a well organised sequence of dynamic regimes: when $v_{\mathrm{LPCwe}} \leqslant v < v_{\mathrm{NSwe}}$ the only stable regime appears to be a limit cycle corresponding to the weave mode (Figure 5); when $v_{\mathrm{NSwe}} \leqslant v \leqslant v_{\mathrm{NSwo}}$ the model exhibits dynamics on torus, with a bimodal frequency spectrum corresponding to a mix of wobble and weave oscillations (Figure 6); when $v > v_{\mathrm{NSwo}}$ the only stable regime appears to be a limit cycle corresponding to the wobble mode (Figure 7).

Note that the oscillations of δ and β on the wobble limit cycle, which exists for $v > v_{\mathrm{NSwo}}$, have roughly constant amplitude at all speeds. In particular, the birth of the stable wobble cycle through a Neimark–Sacker bifurcation implies that wobble appears as a finite and relatively large oscillation from its onset, rather than gradually building up amplitude as velocity increases, as one could expect from the linear analysis in [6]. This supports the empirical observation that shimmy appears as a sudden transition to a large (and scary) high frequency oscillation as the bicycle accelerates.

Figure 9 shows some of the data collected during the same on-road test activity of Figure 1, performed by one of us while riding downhill reaching a speed in the range 12–17 m/s. The inertial measurement unit (IMU) was mounted on the horizontal tube of the bicycle rear frame near the steering axis. Figure 9(a) illustrates the lateral acceleration during a strong shimmy. Initially, oscillations of limited amplitude are probably due to noise and the rolling of the wheels on rough tarmac. At $t \simeq 155$ s oscillations suddenly grow in amplitude, reaching 8 g at $t \simeq 160$ s. Then they disappear at $t \simeq 168$ s. Figure 9(b) shows the signal spectrogram. The frequency peak during shimmy appears as a white horizontal line at $f \simeq 7,5$ Hz: as predicted by our model (see next section), frequency of this peak is independent of the forward speed. The same figure displays a wider-band and lower-frequency spectral component, probably related to weave. The velocity range over which wobble is present is consistent with the results we drew from the above analysis. In Figure 9(c), shimmy oscillations appear when the forward speed v is near v_{NSwo} and disappear when the speed falls below this value. The data, however, suggest the presence of a hysteretic loop (wobble appears at $v \simeq v_{\mathrm{NSwo}}$ but disappears at $v < v_{\mathrm{NSwo}}$). This hysteresis may be explained as a consequence of the relatively high longitudinal acceleration that we observed, during the experiment, as the bicycle was crossing the critical velocity v_{NSwo}. Indeed, the bicycle state may take time to reach the wobble attractor when $v > v_{\mathrm{NSwo}}$, and then to settle onto the stable equilibrium when $v < v_{\mathrm{NSwo}}$. A better understanding of the interplay between acceleration and the structure of these attractors, and of the possible influence of acceleration on the stability of the wobble mode, can however be gained only through further experiments.

3.3. Two-parameter bifurcation analysis

We can gain a more complete understanding of the interplay of the attractors identified in the previous section by analysing how they transform into each other in the two-parameter plane of forward speed v and torsional stiffness coefficient k_β, by looking at the *bifurcation diagram* of Figure 10. We chose to vary k_β in the range $3500 \leqslant k_\beta \leqslant 6000$ Nm/rad, which is a set of realistic values. Note that k_β is a highly uncertain parameter in the model, the

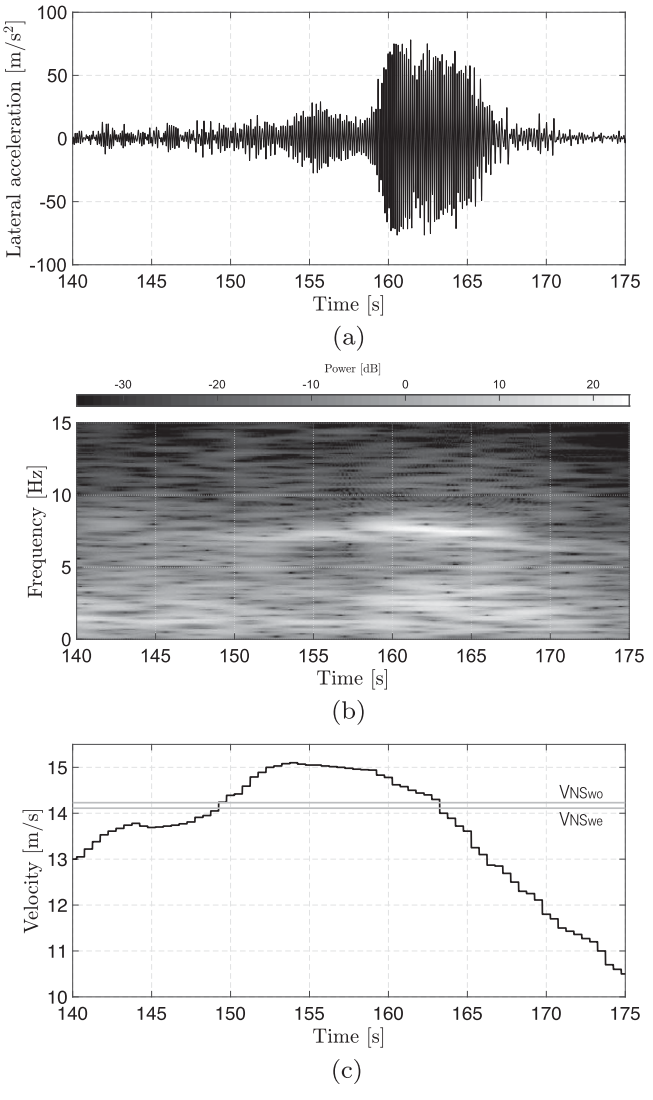

Figure 9. Data recorded during an experimental test activity with the racing bicycle. (a) Lateral acceleration measured on the rear frame near the steering axis, (b) spectrogram, (c) forward speed with v_{NSwe} and v_{NSwo}.

two-parameter analysis provides additional robustness to the conclusions we could draw from the results of the previous section.

The two Hopf curves of weave and wobble, respectively, labelled as H_{we} and H_{wo}, represent the locus of parameter values where the two Hopf bifurcations identified in the previous section occur. We notice that, while H_{we} is nearly vertical (meaning that the weave onset is roughly independent of the torsional stiffness), H_{wo} cuts the parameter plane almost horizontally. This signifies that the onset of the wobble mode is highly dependent on the torsional stiffness parameter, especially at high speed values. The two curves intersect each other in one point that is known as double-Hopf point (HH). As predicted by bifurcation theory [22], two curves of torus bifurcations emanate from the double-Hopf

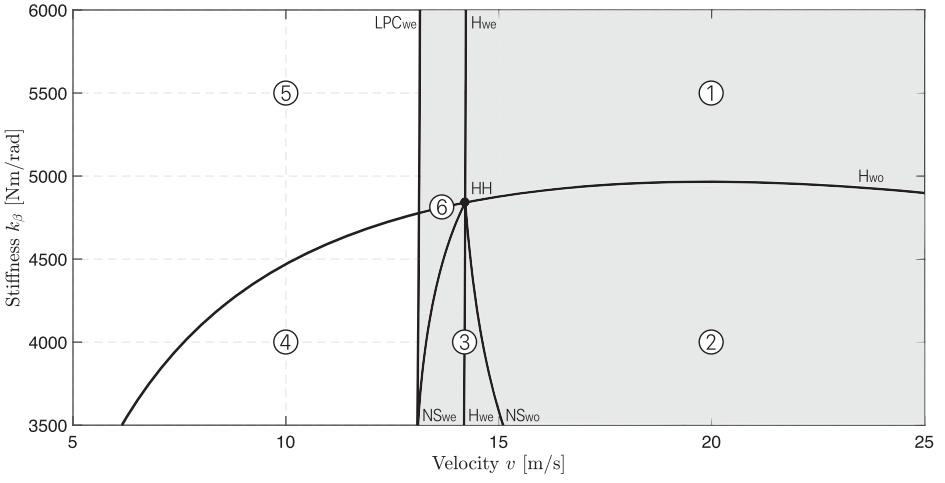

Figure 10. Two-parameter bifurcation diagram in the (v, k_β) plane. Grey areas represent stable motions.

point, NS_{we} and NS_{wo}. These are the Neimark–Sacker bifurcations found in the previous section. Notice that the two NS curves are wider apart as torsional stiffness is decreased. This means that, for lower values of k_β, the speed interval over which we can expect to see an interplay of weave and wobble increases (roughly linearly). The fifth curve in the diagram, labelled as LPC_{we}, is a fold bifurcation of the weave limit cycle, and marks the sudden disappearance of the weave limit cycle (by collision with an unstable cycle) as velocity decreases.

Overall, the bifurcation curves divide the parameter plane into six dynamically different regions. Region ① represents parameter values for which there are no oscillations and the straight, rectilinear motion is stable, meaning that any perturbation decays as t tends to ∞. When the bicycle is inside region ② it is subject to wobble oscillation, that is, high-frequency oscillations of the front frame about the steering axis. This dynamics is related to the presence of stable limit cycles. In region ③ the motion is characterised by the coexistence of both weave and wobble modes and thus the bicycle oscillates on a periodic or quasi-periodic trajectory with two frequency peaks. In region ④ the bicycle is subject to unstable oscillations that bring the vehicle to a fall. Region ⑤, the area inside which the forward speed assumes low value and the torsional stiffness is high, is characterised by an unstable non-oscillating motion. Lastly, in region ⑥ the bicycle is moving with stable oscillations of the rear frame about yaw and roll axes. This is the weave mode of vibration.

Though not displayed in our figures, we investigated the sensitivity of our results to variations (i) in the functional form of Equations (6)–(9), and (ii) in the parameters of the equations.

For the first set of tests (i), we repeated the analysis using a simplified version of the *Magic Formula* in [16] instead of Equations (6)–(9), i.e.:

$$y = D\sin(C\ \arctan(Bx)), \tag{13}$$

where x is the input and can be the side-slip or the camber angles, y represents the lateral force or the aligning torque component, whereas B, C and D are coefficients. The

corresponding stiffness C_{yx} is the derivative of (13) at $x = 0$:

$$C_{yx} = DCB. \tag{14}$$

Equation (14) was used to choose the values of B, C and D to get the stiffness coefficients reported in Table 1. The bifurcation analysis showed no significant change with respect to the diagram in Figure 10. The advantage of using Equations (6)–(9) instead of (13) is that the former require to identify half the coefficients.

For the second set of tests (ii), we evaluated changes in the bifurcation diagram as the parameters of Equations (6)–(9) are changed. First, we modified the saturation values of the four functions, maintaining their slope at small angles unchanged. We noticed that the saturation values mainly affect the amplitude of the weave and wobble cycles, without significant effects on their frequency. Moreover, changes in Equations (6)–(8) appear to have no significant effect on the bifurcation curves in Figure 10. However, when the parameters of Equation (9) are changed to reduce its peak value, without modifying the slope at small angles, we observe a moderate shift of the curve LPC_{we} to the right, and a minor shift of the two Neimark–Sacker curves towards higher values of the stiffness k_β. This suggests that different tyre characteristics, with same small-angle linear coefficients, may affect the amplitudes of the weave and wobble cycles and, to a lower extent, the velocity at which these oscillations appear. A more interesting effect is obtained by rescaling the four functions multiplying them by a factor slightly smaller than one. This reduces their saturation value as well as their slope at small angles, and should correspond to using a softer or less structured tyre. The effect is a downward shift of all the curves in Figure 10. Thus, a slightly less structured tyre appears to have the same beneficial effect as a slightly stiffer frame, moving the system closer or possibly above the H_{wo} curve which marks the boundary of existence of the wobble mode.

Note that the three types of motion from Figures 5–7 are found in Figure 10, respectively, in region ⑥, ③ and ②. The one-parameter bifurcation diagram represented in Figure 8 corresponds to an horizontal cross section of Figure 10 at $k_\beta = 4784.2$ Nm/rad.

Figure 11 shows the variations of weave and wobble peak frequencies as a function of the forward speed and of the torsional stiffness coefficient. The frequency was computed

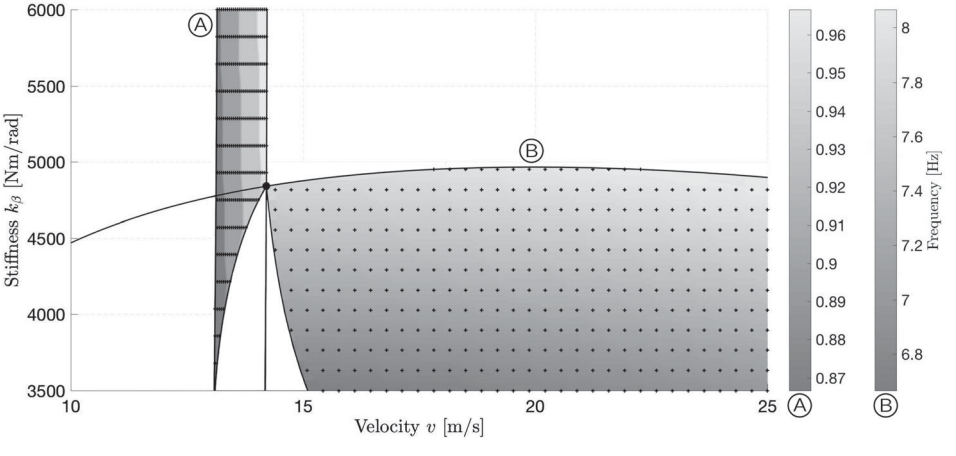

Figure 11. Variations of weave Ⓐ and wobble Ⓑ frequencies in the bifurcation diagram.

by a fast Fourier transform on time simulations performed at the parameter pairs indicated by cross marks. The shaded diagram was then obtained by interpolation and extrapolation of the data. We notice that weave frequency is almost independent of torsional stiffness, while it changes significantly with forward speed: if the cyclist rides faster, weave frequency increases. On the other hand, wobble frequency mainly increases by increasing the torsional stiffness of the frame, while it is only weakly affected by forward speed. This is consistent with Figure 9(b) and with the observations made in [4].

Figure 12 shows the two peak frequencies that characterise bicycle motion between the Neimark–Sacker curves. Even though the two frequencies characterise the same trajectory, their dependence on parameters agrees with the observations above: the weave frequency

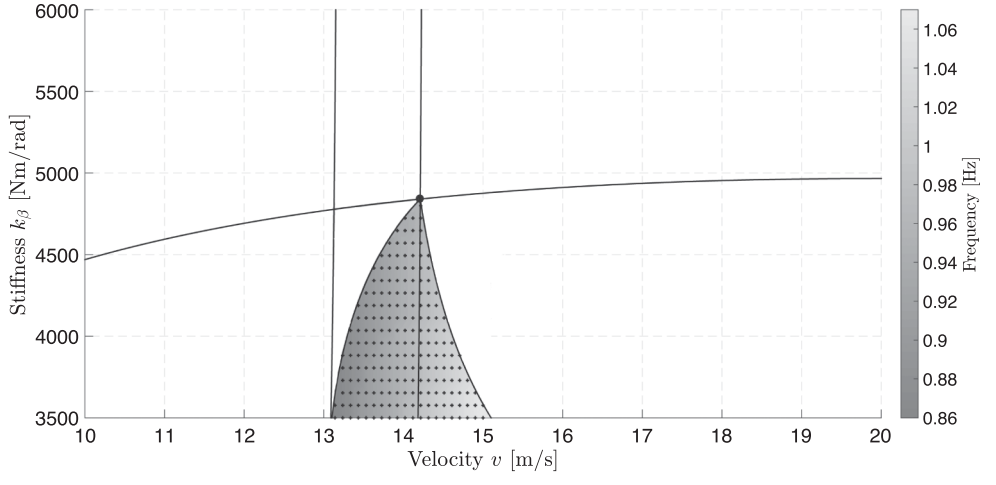

(a)

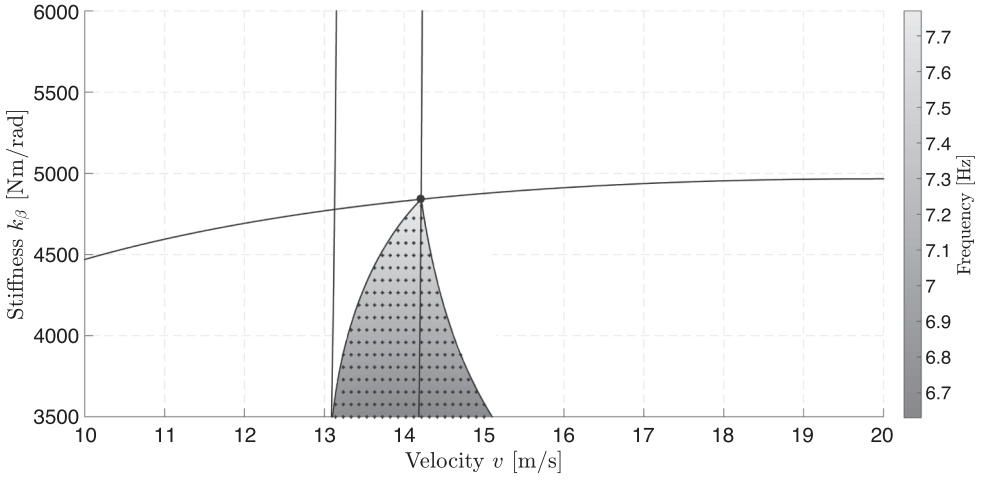

(b)

Figure 12. Variations of motion frequencies in the region where the two vibrational modes are coupled. (a) represents the lower frequency (weave) while (b) shows the higher frequency (wobble).

depends mainly on velocity, the wobble frequency mainly on stiffness. As a consequence, we can conclude that wobble seems to be dependent on structural properties of the racing bicycle, while weave depends mostly on the rider and how fast it is riding.

4. Steering damping

A possible solution to counteract the onset of shimmy is to increase the overall damping about the steering axis, which in our model corresponds to adding an additional damping term c_δ. It can stand for an external shimmy damper or simply for the damping introduced by a rider whose hands firmly hold the handlebar. Figure 13 shows how the bifurcation diagram changes for different damping values. The weave mode remains basically unchanged,

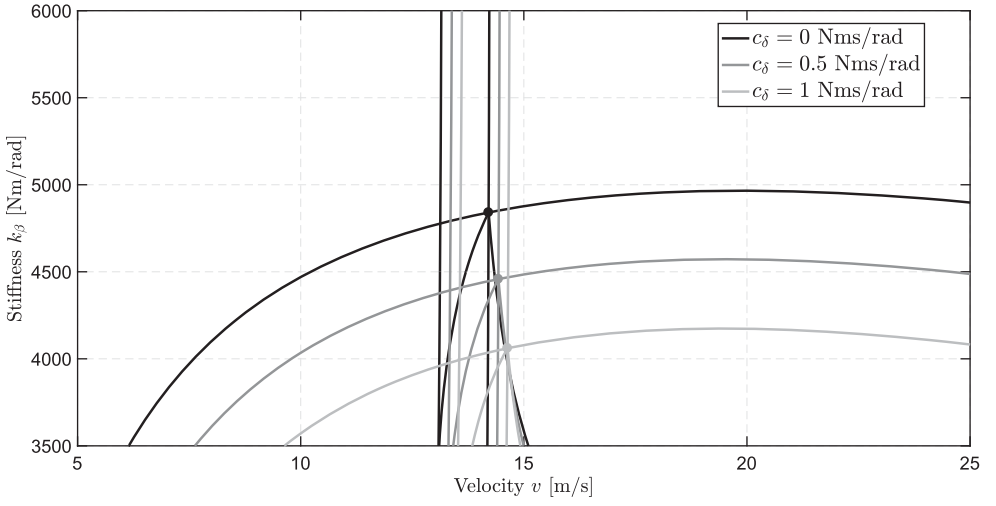

Figure 13. Bifurcation diagram variations for different values of the steering damping c_δ.

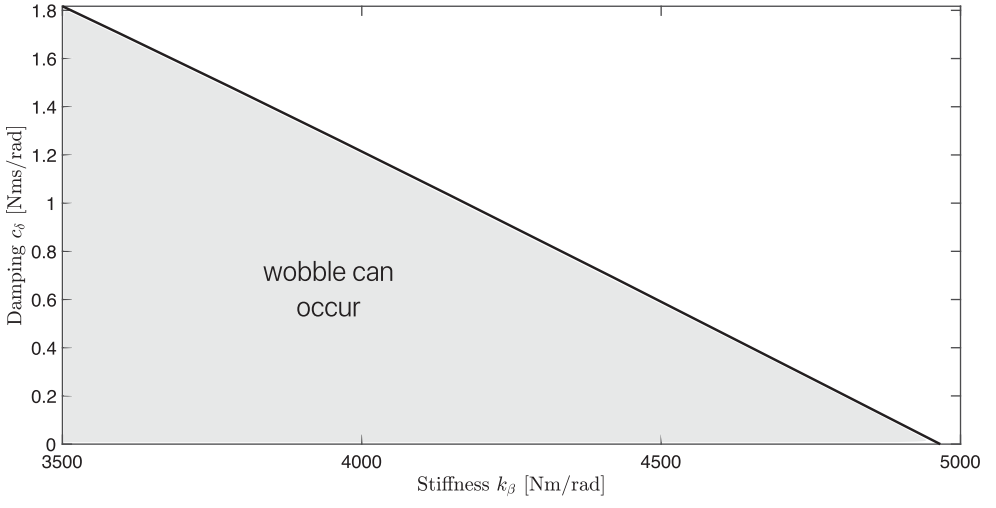

Figure 14. Steering damping c_δ as a function of the frame stiffness k_β. The grey area stands for parameters combinations that can lead to wobble oscillations.

except for a slight shift to the right of its Hopf and LPC curves. The region where wobble occurs (regions ② and ③ in Figure 10) is instead significantly reduced by shifting downward, while the region where the straight, rectilinear motion is stable (region ① in Figure 10) becomes significantly larger. Thus, increasing damping at the steering axis appears to be a more effective measure to eliminate shimmy than increasing torsional stiffness.

These observations are summarised in Figure 14, which shows the maximum k_β value of the curve H_{wo} as a function of the steering damping. In the region below the curve (shaded grey) wobble oscillations occur in some speed interval. Above the curve wobble never appears and, for increasing speed values, the bicycle is subject only to unstable non-oscillating motion, stable weave oscillations and stable motion. For known torsional stiffness k_β, the diagram gives the minimum value of the steering damping c_δ that prevents the onset of shimmy oscillations.

5. Conclusions

In this work the nonlinear dynamics of a 12-dimensional model of a racing bicycle has been analysed. Our objective was to describe the onset and the dynamics of shimmy (wobble) through numerical continuation of equilibria and periodic solutions by varying the forward speed v and the torsional stiffness coefficient k_β. We found that both weave and wobble are stable limit cycles which appear, respectively, at low and high values of the forward speed. In between, however, there is a speed interval in which these two vibrational modes coexist and interact. This behaviour is explained by the presence of a stable torus.

Focusing on shimmy oscillations, their frequency is independent of the forward speed, but depends on structural properties of the bicycle, such as the torsional compliance of the rear frame about the head tube and the possible lateral compliance of the fork and the front hub. Thanks to tyre nonlinear characteristics, these oscillations do not diverge as in the linear model, so they usually do not lead to a fall of the rider. Our model shows that the amplitude of the shimmy limit cycle depends on the saturation values of the four tyre characteristics. A more interesting relation is found between shimmy and the slopes of the tyre characteristics at small angles: a reduced slope, simulating what would happen by using softer or less structured tyres, may altogether prevent the onset of shimmy. This is in accordance with our experience, but a more systematic theoretical and experimental analysis is needed to validate this intuition.

All the results are in agreement with the dataset recorded by one of us riding downhill at high speed with a racing bicycle (this is possibly the first dataset of this kind after [4]). Our model matches the experimental data also in that shimmy appears as a finite and relatively large oscillation from the onset, rather than gradually building up amplitude as the velocity increases. The data, however, displays some hysteresis in the appearance and disappearance of shimmy, which is not present in the model. This hysteresis may be explained as an effect of the bicycle's acceleration at the velocity threshold, though this would have to be verified against further experimental evidence. We are planning to run other on-road experimental activities, to clarify whether the hysteresis is just an effect of the changing velocity, or hides deeper information regarding the model's fine structure.

All in all, the analysis points out that shimmy can be prevented by a rotary viscous damping added to the steering assembly or by using different tyres and, more importantly, allows

to quantify the relation between damping, tyre characteristics, and the wobble amplitude. Otherwise, if a violent shimmy occurs while riding, the only effective remedy is to try to reduce the forward speed. According to our experience, this can be achieved by gently using the rear brake and by raising the upper body to increase the aerodynamic drag.

Notes

1. The camber angle γ is defined as the angle between the wheel centre plane and a vertical axis, while the side-slip angle α is the angle between the wheel centre plane and the direction of the wheel forward velocity.
2. Equations (4) and (5) appear in [6] with slightly different notation.
3. Following the terminology from [21], we call supercritical a Hopf bifurcation where the first Lyapunov coefficient has negative sign. This implies that the limit cycle generated from the Hopf bifurcation is stable *restricted to the centre manifold*.

Disclosure statement

No potential conflict of interest was reported by the authors.

Notes on contributors

Nicolò Tomiati received the B.S. degree and the M.S. degree in aerospace and aeronautical engineering from Politecnico di Milano, Milan, in 2014 and 2016, respectively. From 2017, he has been a researcher at the Department of Electronics, Information and Bioengineering (DEIB) of Politecnico di Milano. His research interests include bicycle dynamics focused on shimmy, vibrations, nonlinear dynamics, and modeling and simulation of multi-body systems.

Alessandro Colombo received the Diplôme D'Ingénieur from ENSTA in Paris in 2005, and the Ph.D. from Politecnico di Milano in 2009. He was Postdoctoral Associate at the Massachusetts Institute of Technology in 2010–2012, and he is currently Assistant Professor in the Department of Electronics, Information and Bioengineering at Politecnico di Milano. His research interests are in the analysis and control of nonlinear, discontinuous, and hybrid systems.

Gianantonio Magnani is a professor of Automatic Control and Robotics at Politecnico di Milano. He has published more than a hundred papers in international Journals and conference proceedings. He is an avid user of two wheel vehicles, and he started his studies on shimmy after experimenting it in a fast downhill with a race bicycle in 2010.

ORCID

Nicolò Tomiati http://orcid.org/0000-0003-2259-8608

References

[1] Brandt J. Shimmy or speed wobble [cited 2004 Jun]. Available from: http://www.sheldonbrown.com/brandt/shimmy.html
[2] Rinard D. Bicycle shimmy or speed wobble [cited 2007 Sept]. Available from: https://www.youtube.com/watch?v=xODNzyUbIHo
[3] Empfield D. Speed wobble [cited 2015 Apr]. Available from: http://www.slowtwitch.com/Tech/SpeedWobble5033.html
[4] Magnani G, Papadopoulos J, Ceriani NM. On-road measurements of high speed bicycle shimmy, and comparison to structural resonance. Proceedings of the IEEE international conference on mechatronics (ICM); 2013 Feb 24–Mar 1; Vicenza, IT; 2013. p. 400–405.

[5] Nusime J, Klinger F, Edelmann J, et al. Some considerations on modelling bicycle wobble at high speed. Proceedings of bicycle and motorcycle dynamics; 2013 Nov 11–13; Narashino, Japan; 2013.
[6] Klinger F, Nusime J, Edelmann J, et al. Wobble of a racing bicycle with a rider hands on and hands off the handlebar. Veh Syst Dyn. 2014;52(Suppl 1):51–68 [cited 2017 Oct 12]. Available from: http://dx.doi.org/10.1080/00423114.2013.877592
[7] Meijaard J, Papadopoulos JM, Ruina A, et al. Linearized dynamics equations for the balance and steer of a bicycle: a benchmark and review. Proc R Soc Lond A. 2007;463(2084):1955–1982 [cited 2017 Sep 25]. Available from: http://rspa.royalsocietypublishing.org/content/463/2084/1955.
[8] Spierings PTJ. The effects of lateral front fork flexibility on the vibrational modes of straight-running single-track vehicles. Veh Syst Dyn. 1981; 10(1):21–35 [cited 2017 Nov 2]. Available from: http://dx.doi.org/10.1080/00423118108968633.
[9] Sharp RS. A brief commentary on the paper 'The effects of lateral front fork flexibility on the vibrational modes of straight-running single-track vehicles' by Spierings PTJ. Veh Syst Dyn. 1981;10(1):37–38 [cited 2017 Sept 15]. Available from: http://dx.doi.org/10.1080/00423118108968634.
[10] Sharp RS, Alstead CJ. The influence of structural flexibilities on the straight-running stability of motorcycles. Veh Syst Dyn. 1980;9(6):327–357 [cited 2017 Oct 3]. Available from: http://dx.doi.org/10.1080/00423118008968629.
[11] Plöchl M, Edelmann J, Angrosch B, et al. On the wobble mode of a bicycle. Veh Syst Dyn. 2012;50(3):415–429 [cited 2017 Oct 24]. Available from: http://dx.doi.org/10.1080/00423114.2011.594164.
[12] Pacejka HB. Analysis of the shimmy phenomenon. Proc Inst Mech Eng. 1965;180(1):251–268.
[13] Tomiati N, Magnani G, Scaglioni B, et al. Model based analysis of shimmy in a racing bicycle. Proceedings of the 12th international modelica conference; 2017 May 15–17; Prague, Czech Republic; 2017. p. 441–447.
[14] Meijaard JP, Popov AA. Numerical continuation of solutions and bifurcation analysis in multibody systems applied to motorcycle dynamics. Nonlinear Dyn. 2006;43(1):97–116 [cited 2017 Sep 20]. Available from: https://doi.org/10.1007/s11071-006-0753-y.
[15] Doria A, Favaron V, Roa S. A doe approach for evaluating the effect of bicycle properties on stability. Proceedings of the ASME 2017 international design engineering technical conferences and computers and information in engineering conference; 2017 Aug 6–9; Cleveland, Ohio, USA; 2017.
[16] Pacejka HB. Tire and vehicle dynamics. 3rd ed. Oxford: Butterworth-Heinemann; 2012.
[17] Limebeer DJN, Sharp RS. Bicycles, motorcycles and models. IEEE Control Syst Mag. 2006;26:34–61.
[18] Doria A, Tognazzo M, Cusimano G, et al. Identification of the mechanical properties of bicycle tyres for modelling of bicycle dynamics. Veh Syst Dyn. 2013;51(3):405–420 [cited 2017 Oct 13]. Available from: http://dx.doi.org/10.1080/00423114.2012.754048.
[19] Dressel A, Papadopoulos J, Schwab AL. Bicycle tire measurements and steady-state models, for use in vehicle dynamic simulations. In: Gruber P, Sharp RS, editors. Proceedings of the 4th international tyre colloquium; 2015 Apr 20–21; Guildford, UK; 2015. p. 118–120.
[20] Dhooge A, Govaerts W, Kuznetsov YA, et al. New features of the software matcont for bifurcation analysis of dynamical systems. Math Comput Model Dyn Syst. 2008;14(2):147–175 [cited 2017 Oct 4]. Available from: https://doi.org/10.1080/13873950701742754.
[21] Kuznetsov Y. Elements of applied bifurcation theory. 3rd ed. New York: Springer; 2004.
[22] Guckenheimer J, Holmes PJ. Nonlinear oscillations, dynamical systems and bifurcations of vector fields. New York: Springer; 1983.